forests

MDPI

Article

Shelter Effect of Pedestrian Wind behind Row Trees in a Line Arrangement

Fuh-Min Fang [1], Jen-Chieh Chang [1], Yi-Chao Li [2], Cheng-Yang Chung [3] and Ming-Hsun Chan [4,*]

[1] Department of Civil Engineering, National Chung Hsing University, Taichung City 403302, Taiwan; fmfang@nchu.edu.tw (F.-M.F.); dose0212@yahoo.com.tw (J.-C.C.)
[2] Taiwan Building Technology Center, National Taiwan University of Science and Technology, Taipei City 106335, Taiwan; liyichao@mail.ntust.edu.tw
[3] Aerospace Science and Technology Research Center, National Cheng Kung University, Tainan City 701401, Taiwan; scychung@mail.ncku.edu.tw
[4] Department of Forestry and Natural Resources, National Chiayi University, Chiayi 60004, Taiwan
* Correspondence: mhchan@mail.ncyu.edu.tw; Tel.: +886-5-2717466

Abstract: Flow past a single-line arrangement of evenly-spaced row trees, in an open territory, was numerically simulated under the action of a boundary-layer type of oncoming flow, with a strength of "strong breeze", based on the Beaufort scale. By selecting *Koelreuteria henryi* as the demonstrated tree species, the spatial wind speed variations behind row trees at the pedestrian level, at various tree heights and tree spaces, were analyzed to investigate the corresponding downstream shelter effects from a systematic basis. Based on the results of the analyses, the tendency of stream-wise wind speed variations behind the row trees was presented so as to provide additional insights into row-tree planning for protection against ground wind. Moreover, in other cases of row trees with similar crown shapes and properties, resulting flow fields for various tree heights and tree spaces can provide referable quantitative information, which can be readily used to conduct tentative shelter effect assessments and pedestrian comfort evaluations in a preliminary planning stage.

Keywords: row trees; shelter effect; pedestrian wind; numerical simulations

check for updates

Citation: Fang, F.-M.; Chang, J.-C.; Li, Y.-C.; Chung, C.-Y.; Chan, M.-H. Shelter Effect of Pedestrian Wind behind Row Trees in a Line Arrangement. *Forests* **2022**, *13*, 392. https://doi.org/10.3390/f13030392

Academic Editor: Chi Yung Jim

Received: 10 January 2022
Accepted: 25 February 2022
Published: 27 February 2022

Publisher's Note: MDPI stays neutral with regard to jurisdictional claims in published maps and institutional affiliations.

Copyright: © 2022 by the authors. Licensee MDPI, Basel, Switzerland. This article is an open access article distributed under the terms and conditions of the Creative Commons Attribution (CC BY) license (https://creativecommons.org/licenses/by/4.0/).

1. Introduction

Planting trees can improve the view of a landscape and also affect local ground wind conditions. In addition to improving the view of a local landscape, the existence of trees can also lead to a reduction in downstream near-ground wind speeds, thus improving the improving human comfort and can even improve safety in the context of gust of winds.

The technique of planting row trees had been frequently employed for wind protection in windy areas of Taiwan. A practical example can be found at Budai Port on the south-western coast of Taiwan (see Figure 1). To shelter the harbor pool region from strong winds during the fall and winter seasons, row trees were planned to be placed at the periphery of the protected region. Although landscape planners generally realize that both the local appearance and wind fields should be taken into account to determine the type of row-tree arrangement, an evaluation of the precise efficiency of ground wind reduction is considered to be difficult due to a lack of quantitative wind data to refer to.

Generally, wind fields in an open space with trees can vary according to local meteorology and ground features, such as surface roughness and the topology of terrains. In addition to the strength and patterns of oncoming wind flows, existing plants can also affect the local spatial wind-flow fields. Since parts of tree crowns are porous and allow for penetration, downstream wind flow behaves differently from the case of a non-penetrable body. Due to its complicated nature, the analysis of wind behavior behind trees has become an important task to address at the planning stage of tree planting.



Figure 1. Area for wind protection at Budai Port in Taiwan.

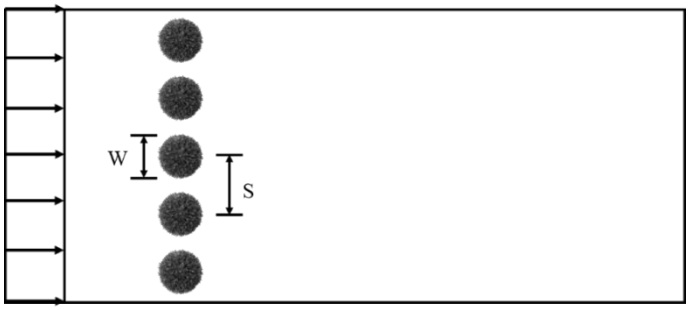
2. Goal and Description of Study

By taking a simplified row-tree problem for ground-wind protection using a commonly adopted species of tree as the demonstrated case, the goal of this study is two-fold: to explore the general behavior and features of flows behind row trees to assist landscape planners, and to investigate the effects of flows behind row trees due to changes in tree heights and tree spaces to achieve general principles for the selection of row-tree arrangements.

Figure 2 illustrates a schematic of the problem. A series of numerical flow simulations were conducted to investigate near-ground wind flow behind a line arrangement of evenly-spaced row trees, in an open and flat area, at various tree heights (H = 6 m, 9 m, 12 m and 15 m) and tree spacings (S = 1.2 W, 1.5 W and 1.8 W; W is the tree crown width) on a systematic basis. The resulting downwind flow fields at a pedestrian level were further analyzed to explore the features and tendencies of stream-wise wind speed variations behind trees.



(**a**) Side view



(**b**) Top view

Figure 2. Schematic of the study.

In the study, the oncoming wind flow direction was perpendicular to the line of row trees. The pattern of the oncoming wind flow was set as a boundary-layer type with a ground condition subject to type C exposure, which is considered typical in common

developing territories. According to the ASCE/SEI 7-16 [1] wind code, the corresponding gradient height and power-law α value of the oncoming wind flow are 300 m and 0.15, respectively. The strength of the oncoming flow was chosen to be a number 6 flow (strong breeze), based on the Beaufort scale.

In numerical computations, a k-ε turbulence model was employed to reflect the existing turbulence characteristics of the wind flows. Since tree crowns allow for wind penetrations, they were treated as porous media. In the porous parts of the simulated wind field, appropriate source terms were included in the associated governing equations to physically describe the penetrating behavior of the wind flow. Furthermore, to correctly simulate the retardation effect associated with tree crowns, certain tree factors, which reflect the retardation effect of the penetrable crown, had to be determined before the numerical computations were executed. In this study, values were obtained based on the comparisons between the measured wind velocity profiles downstream of a model tree in wind tunnel experiments and the predicted values.

3. Related Studies

A number of previous related studies have focused on the areas of forestry and meteorology. Using field observations, the major focus was to examine the global wind flow characteristics of trees in forests. Many originally 3-D wind-flow problems were simplified into 2-D or even 1-D cases. Finnigan [2] pointed out that surface wind flow regions could be divided into a canopy and a surface sublayer. Based on the results of field observations, Raupach et al. [3] found that the turbulent flow pattern within the canopy sublayer was similar to that of a mixing-layer flow. By performing wind tunnel experiments, Raupach et al. [4] proposed a description of the wind speed profile in forest territories. Mihailovic et al. [5] also suggested similar profiles. According to the results of wind tunnel measurements, Massman [6] used the concept of leaf area index (LAI). Certain discussions were made regarding its influences, such as the wind speed profiles, surface shear velocities, and roughness heights. Moreover, Novak et al. [7] concluded that a change in the spatial density of forest trees could affect the characteristics of local mean and turbulent flows, which are mainly dominated by large-scale turbulence eddies. In a wind tunnel study of wind flows past a single layer and a double layer of plants, Boldes et al. [8] found that mixing flows occurred in the wake region and produced bleed flows due to the effects of large-scale eddies. Further experimental works were performed by Flesch and Wilson [9,10] to investigate the extent of wind speed reduction downstream of tree groups and the resulting protected area.

On the other hand, there are also several studies on numerical predictions of wind flow around trees. Since full descriptions of the geometries of twigs and leaves in tree crowns involve a large amount of computing time, these were considered inefficient in the execution of numerical flow computations. Uno et al. [11] proposed a second-order turbulence model to study the role of the urban canopy layer in the formation of a nocturnal urban boundary layer. Based on the eddy-viscosity concept, Hiraoka [12] adopted ensemble-averaging and spatial averaging techniques to simulate flows within plant and urban canopies. Shaw and Schumann [13] proposed the inclusion of appropriate source terms in the momentum equations in flow simulations of the spatial parts of tree crowns, to physically reflect the penetration features of crowns. The introduced drag terms were the overall outcome of the drag coefficient, leaf density, and combined velocities. Moreover, Wilson and Flesch [14] employed a 2-D numerical model to simulate flow fields in forests. In comparison, the predicted wind speed profiles agreed well with the in-field results. Moreover, Su et al. [15] performed large eddy simulations (LES) to successfully predict neutrally stratified flows past forests. Moreover, LES computations were also carried out by Patton and Davis [16] to investigate the dispersion mechanism of chemicals in forests. Further, Watanabe [17] also performed large eddy computations to examine the turbulence structure of wind flows above forests. In addition, Sládek et al. [18] numerically investigated the 2-D and 3-D wind fields of boundary-layer flows past forests in areas with complex topography, based on

a k-ε turbulence model. More recently, Fang et al. [19] extended the ideas of Shaw and Schumann [13] to simulate flows around discrete coniferous trees. By combining the drag coefficient (C_D) and leaf area index (LAI), a factor (C_{Da}) was introduced to reflect the overall wind retardation effect of tree crowns. The predicting flow fields behind discrete trees compared well with measurement results.

4. Numerical Method

Ansys FLUENT software was used to perform the wind flow predictions. Essentially, the governing equations of the solver associated with the incompressible turbulent flows was in a RANS (Reynolds-averaged Navier–Stokes) form. The reliable k-ε model was selected to solve the transport equations of turbulence kinetic energy (k) and the dissipation rate (ε) to further achieve the corresponding distribution of turbulent viscosity (ν_t).

Generally, the Reynolds-averaged continuity and momentum equations are:

$$\nabla \cdot \vec{u} = 0, \tag{1}$$

$$\frac{\partial \vec{u}}{\partial t} + (\vec{u} \cdot \nabla)\vec{u} = -\frac{1}{\rho}\nabla p + \vec{g} + (\nu + \nu_t)\nabla^2 \vec{u}, \tag{2}$$

where $\vec{u}$ is the time-averaged velocity vector and t represents time. p, ρ, and ν are respectively time-averaged pressures, density, and kinematic viscosity of air. $\vec{g}$ is gravity.

After solving the transport equations of turbulent kinetic energy (k) and dissipation rate (ε) in index forms:

$$\frac{\partial k}{\partial t} + u_j \frac{\partial k}{\partial x_j} = \frac{\partial}{\partial x_j}\left(\frac{\nu_t}{\sigma_k}\frac{\partial k}{\partial x_j}\right) + \nu_t\left(\frac{\partial u_i}{\partial x_j} + \frac{\partial u_j}{\partial x_i}\right)\frac{\partial u_i}{\partial x_j} - \varepsilon, \tag{3}$$

$$\frac{\partial \varepsilon}{\partial t} + u_j \frac{\partial \varepsilon}{\partial x_j} = \frac{\partial}{\partial x_j}\left(\frac{\nu_t}{\sigma_\varepsilon}\frac{\partial \varepsilon}{\partial x_j}\right) + C_{1\varepsilon}\frac{\varepsilon}{k} - C_{2\varepsilon}\frac{\varepsilon^2}{k}, \tag{4}$$

with $C_{1\varepsilon}$ = 1.44, $C_{2\varepsilon}$ = 1.92, and turbulent Schmidt numbers σ_k = 1.0 and σ_ε = 1.2, the turbulent diffusivity (ν_t) is then obtained as:

$$\nu_t = C_\mu \frac{k^2}{\varepsilon}. \tag{5}$$

In the spatial part of tree crowns, particularly, certain source terms are added in the associated governing equations to reflect the corresponding retardation effects. In the momentum equation, the additional source term adopts the suggestions of Shaw and Schumann [13] and Fang et al. [19] as:

$$S_m = -C_{Da}\, u_i \vec{u} \tag{6}$$

with $C_{Da} = C_D \times a$, where C_D is drag coefficient and "a" is leaf area index (LAI) of the tree crown.

According to the suggestion of Uno et al. [11], the additional source terms in the k and ε transport equations, in index form, s are, respectively:

$$S_k = u_i S_m, \tag{7}$$

$$S_\varepsilon = 1.5\frac{\varepsilon}{k} S_k, \tag{8}$$

In Ansys FLUENT, the treatment of the additional source terms can be addressed by including appropriate user-defined functions (UDF) during program executions. It is also noted that factor C_{Da} is related to the spatial densities of leaves and twigs in tree crowns. According to the work of Fang et al. [19], this factor can be obtained by experiments.

5. Selection of Tree Type

As *Koelreuteria henryi* is one of the most popular native landscape trees adopted for row trees planting in Taiwan (see Figure 3), it was selected as the target tree species in the present study. Accordingly, a number of images of *Koelreuteria henryi* were collected through field observations to estimate their shapes and crown densities, according to the evaluation procedures suggested by Schomaker et al. [20]. The final tree shape and related properties, such as the crown density, were the averaged outcomes of the observed results from different observers.



Figure 3. Picture of *Koelreuteria henryi*.

6. Determination of C_{Da} Value

Wind tunnel experiments were conducted at the Architecture and Building Research Institute (ABRI) in Taiwan. A model tree was set on the tunnel floor of a test section (6.6 m in width and 2.6 m in height) for downstream velocity measurements. The model tree, including a trunk, twig, and leaves, was produced using a 3-D printer. After the tree model was completed, further estimates of its crown density were repeated according to the same procedure of Schomaker et al. [20], to ensure that the crown density of the model tree agreed with the observed averaged values of *Koelreuteria henryi*.

Figure 4 depicts the shape and dimensions of the tree model. Considering the consistency of the analysis results, the tree was made in an axi-symmetrical shape. Table 1 illustrates its related properties. This model tree was taken as the standard one to perform the following numerical wind flow analyses.

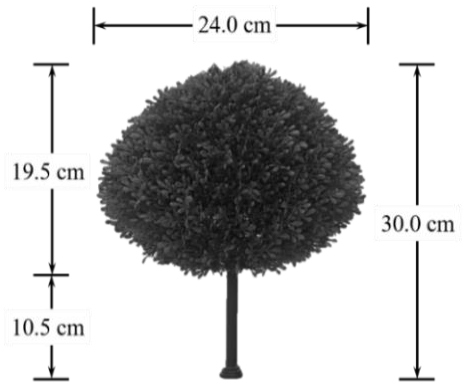


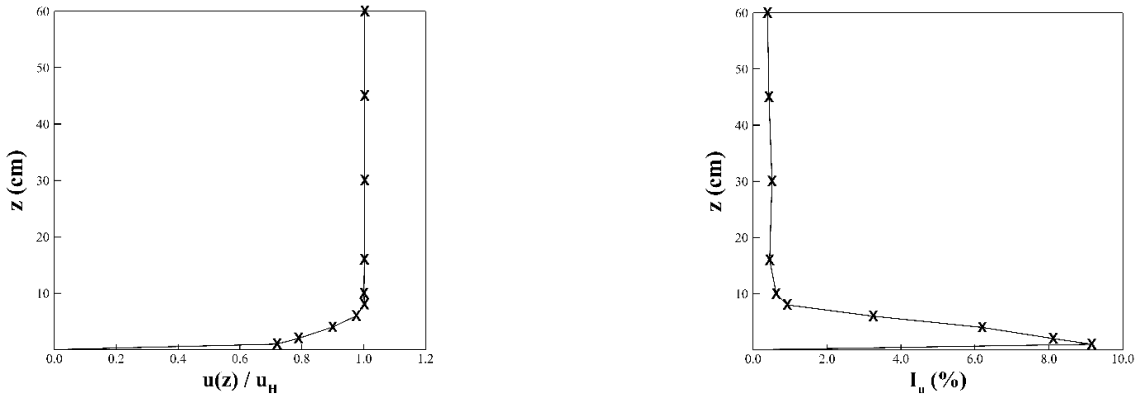
Figure 4. Schematic of the model tree.

Table 1. General properties of the model tree.

Item	
Tree height (H)	30.0 cm
Crown length (L)	19.5 cm
Crown width (W)	24.0 cm
Height of crown base	10.5 cm
Crown density [1]	80%
Crown ratio (L/H) [1]	65%
Leaf area index [2]	1.44

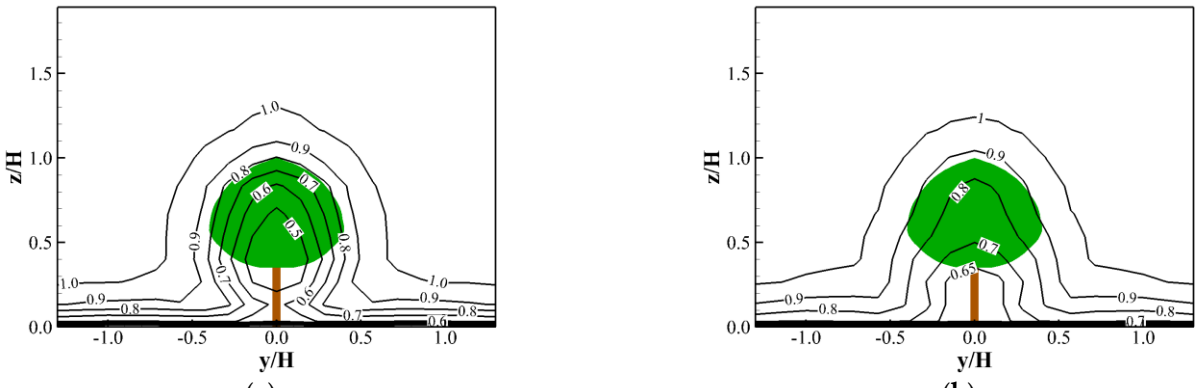
[1] According to the USDA-suggested procedure of Schomaker at al. [20].[2] Measured by LI-COR LAI-2000 Plant Canopy Analyzer.

Figure 5 shows the mean velocity and turbulent intensity (I_u) profiles of the oncoming flow in the wind tunnel experiments (u_H = 8.10 m/s). A TFI Cobra probe was set downstream of the tree to measure the velocity profiles at 3 H and 4.5 H, respectively, downstream. A Cobra probe is a multi-hole pressure probe that provides dynamic three-component real-time velocity measurements. It is capable of a linear frequency-response from 0 Hz to more than 2 kHz, and is available in various ranges of use, between 2 m/s and 100 m/s. In all the velocity measurements, the sampling rate was 1000 Hz and the measurement period was 64 s. Figure 6 illustrates the measured downstream velocity profiles.



(**a**) Mean velocity (**b**) Turbulent intensity profile

Figure 5. Velocity profiles of the oncoming flow in the experiments.



(**a**) (**b**)

Figure 6. Measured mean velocity profiles at (**a**) x = 3 H and (**b**) x = 4.5 H.

Parallel flow simulations were conducted using a number of tentative selections of the crown factors (C_{Da}). By comparing the predicted downstream velocity profiles with

the measured ones, the C_{Da} value, leading to the best agreement, was then determined. Figure 7 shows the variations of the resulting normal root-mean-square error (NRMSE), or the average relative error, in relation to the change in C_{Da} value. Accordingly, the best C_{Da} value was obtained at 0.86. The resulting relative errors of the downstream flow predictions were less than 4.2%. Figure 8 shows the corresponding predicted downstream velocity profiles.

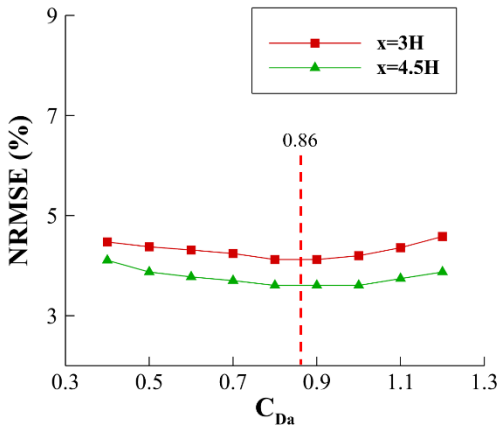


Figure 7. Variation of normal root-mean-square errors.

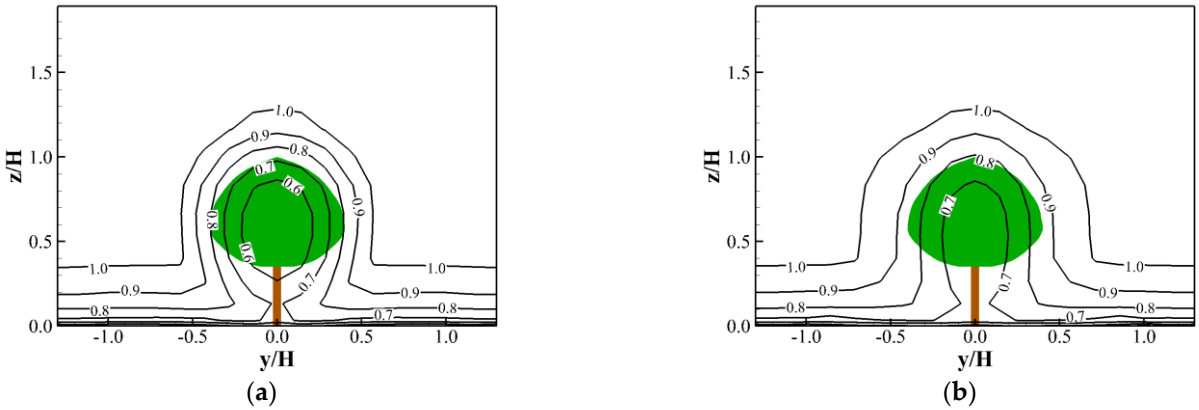


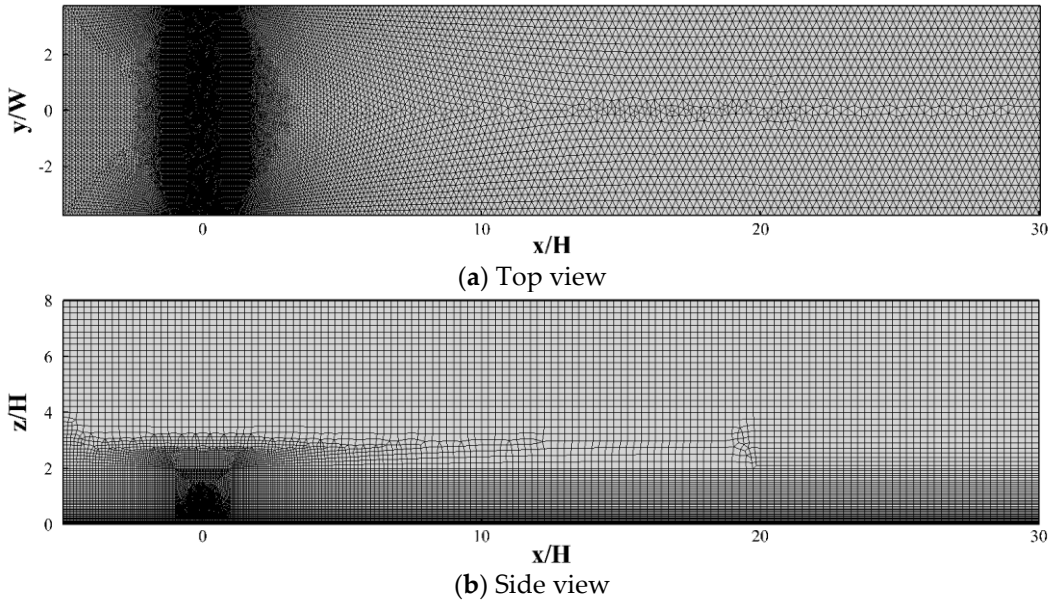
Figure 8. Predicted mean velocity profiles at (**a**) x = 3 H and (**b**) x = 4.5 H (C_{Da} = 0.86).

7. Numerical Predictions of Wind Fields around Row Trees

After the C_{Da} value associated with the standard tree was determined, a series of numerical flow computations were conducted in an open flat area with a line of evenly-spaced row trees of various tree heights (H = 6 m, 9 m, 12 m, 15 m) and at various tree spacings (S = 1.2 W, 1.5 W, 1.8 W; W is crown width) of row trees to examine the resulting shelter effects from the trees. As a rural territory was considered, C exposure [1] was selected for the ground condition. The shape of the velocity profile of the oncoming flow was in a boundary-layer type with a boundary-layer thickness (δ) equal to 300 m and a power-law α value of 1.5 [1]. The strength of the oncoming flow was chosen as number 6 (strong breeze), based on the Beaufort scale. In particular, wind speeds at 10 m and 2 m above ground were, respectively, 11.0 and 8.64 m/s.

In the numerical computations, it was assumed that trees remained the same geometric shape and had the same crown density as that of a standard tree (see Figure 1 and Table 1). That is, the related dimensions of the tree, such as crown length and crown width, were in fixed proportions to the tree height. Moreover, trees were considered rigid. That is, the effect of tree defections and motions due to the action of wind were not considered in the flow analyses.

Figure 9 illustrates the computation domain in a typical case were the tree height (H) was 6 m and the tree spacing (S) was 1.5 W. The dimensions of the rectangular computation domain were 35 H, 6.4 H (or 8 W) and 8 H, respectively, in the along-wind (x), across-wind (y), and vertical (z) directions. Figure 9 also shows the unstructured grid system used in the flow computations. The total number of the grids was nearly three million. The minimum volume of the grid was 4.7×10^{-5} m^3. An additional examination of the flow simulations was conducted using a larger computation domain (60 H × 9.6 H × 12 H). The comparison of the calculated results indicated that the relative difference of the predicted results was within 3%.



(**a**) Top view

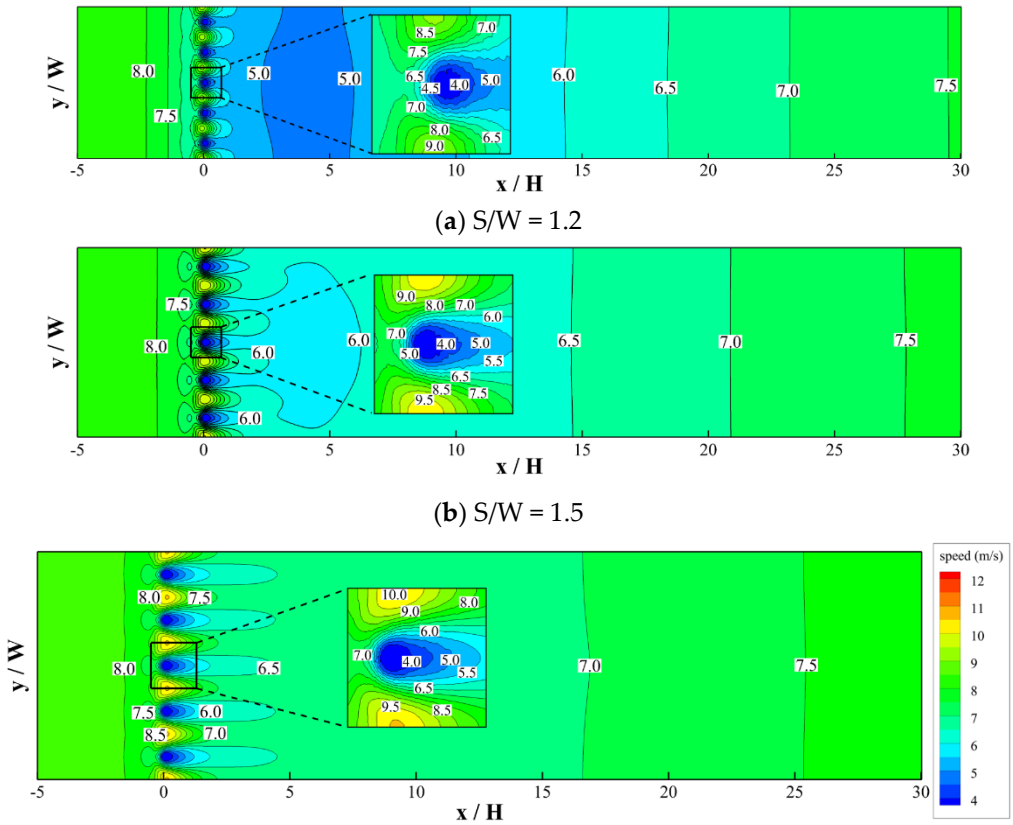
(**b**) Side view

Figure 9. Computational domain and grid system (H = 6 m, S/W = 1.5).

Appropriate values of pressures, velocities, k, and ε were specified at the boundaries of the computational domain to reflect their physical natures. At the ground, a no-slip condition was used. At the upstream inlet section, a power-law velocity profile was imposed. In addition, zero-gradient specifications were employed at the side boundaries and at the downstream end.

8. Results

Based on the numerical results, Figures 10–13 illustrate the wind speed contours at different tree heights (H) and tree spaces (S) at a ground level of 2 m, corresponding to a common upper limit for pedestrians. Generally, the tendency of wind speed variations at the pedestrian level shows that, as the oncoming flow approaches the trees, it tends to slow down. Lower velocities occur in part of the crowns. In the void spaces between trees, on the other hand, air flow is squeezed and speeds up. As a result, significant spatial deviations in wind speed patterns were found immediately behind the row trees. Further downstream, the extent of the speed deviation along the across-wind direction becomes milder, mainly due to the effect of flow mixing. In addition, wind speed gradually increases at greater downstream distances behind the trees. Figures 8–11 also reveal that when tree space (S) or tree height (H) increases, the extent of across-wind velocity deviation becomes more significant and the overall downstream wind speeds tend to increase.

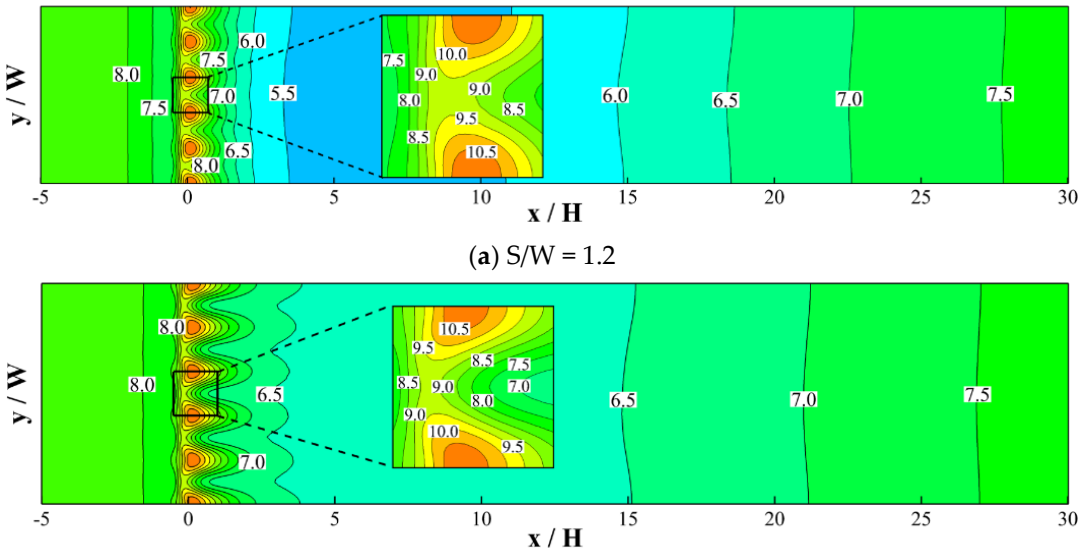


(**a**) S/W = 1.2

(**b**) S/W = 1.5

(**c**) S/W = 1.8

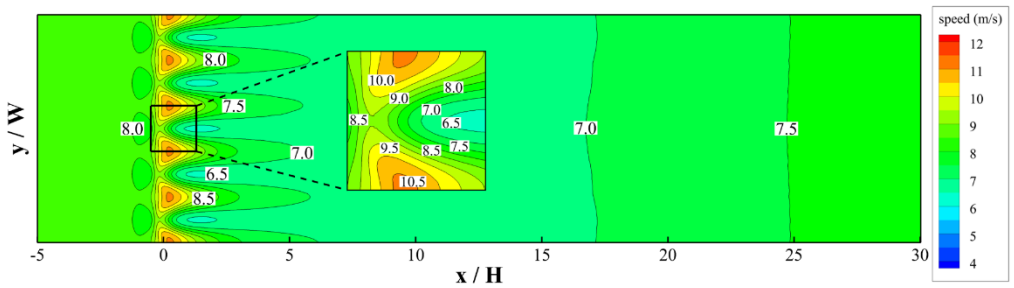
Figure 10. Pedestrian wind speed contours for different tree spaces (H = 6 m).



(**a**) S/W = 1.2

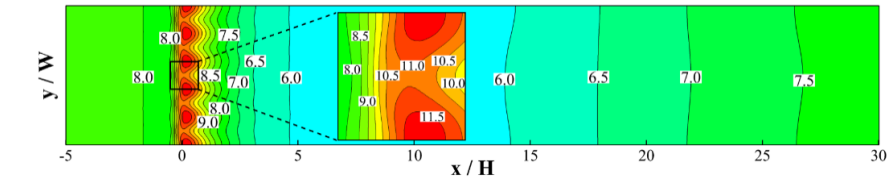
(**b**) S/W = 1.5

Figure 11. *Cont.*

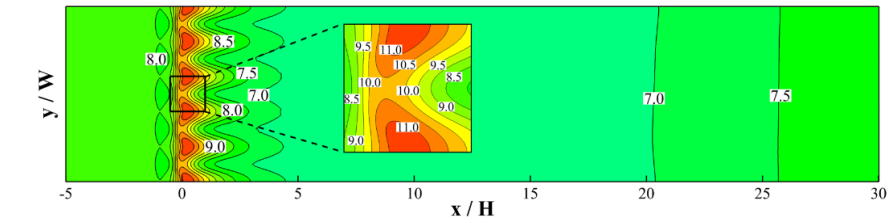


(**c**) S/W = 1.8

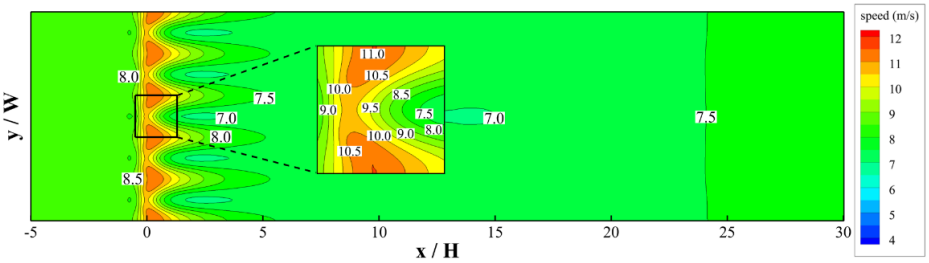
Figure 11. Pedestrian wind speed contours for different tree spaces (H = 9 m).



(**a**) S/W = 1.2

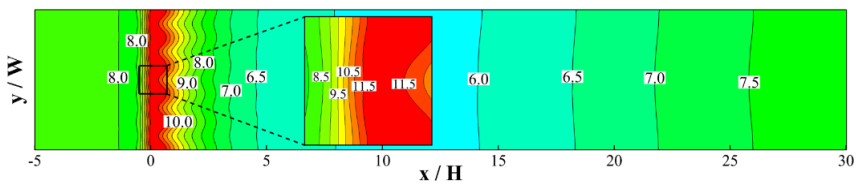


(**b**) S/W = 1.5

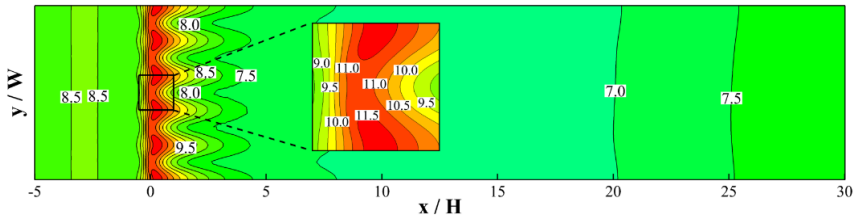


(**c**) S/W = 1.8

Figure 12. Pedestrian wind contours for different tree spaces (H = 12 m).

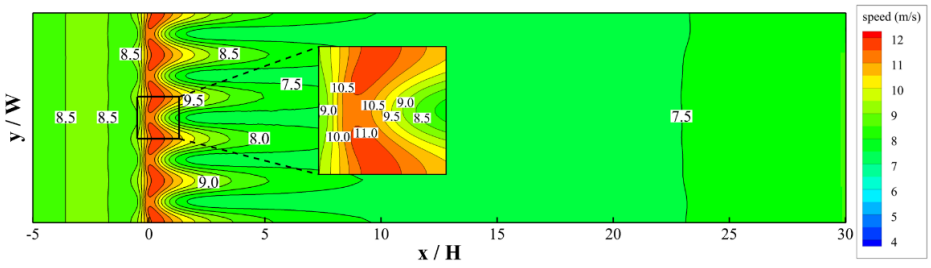


(**a**) S/W = 1.2



(**b**) S/W = 1.5

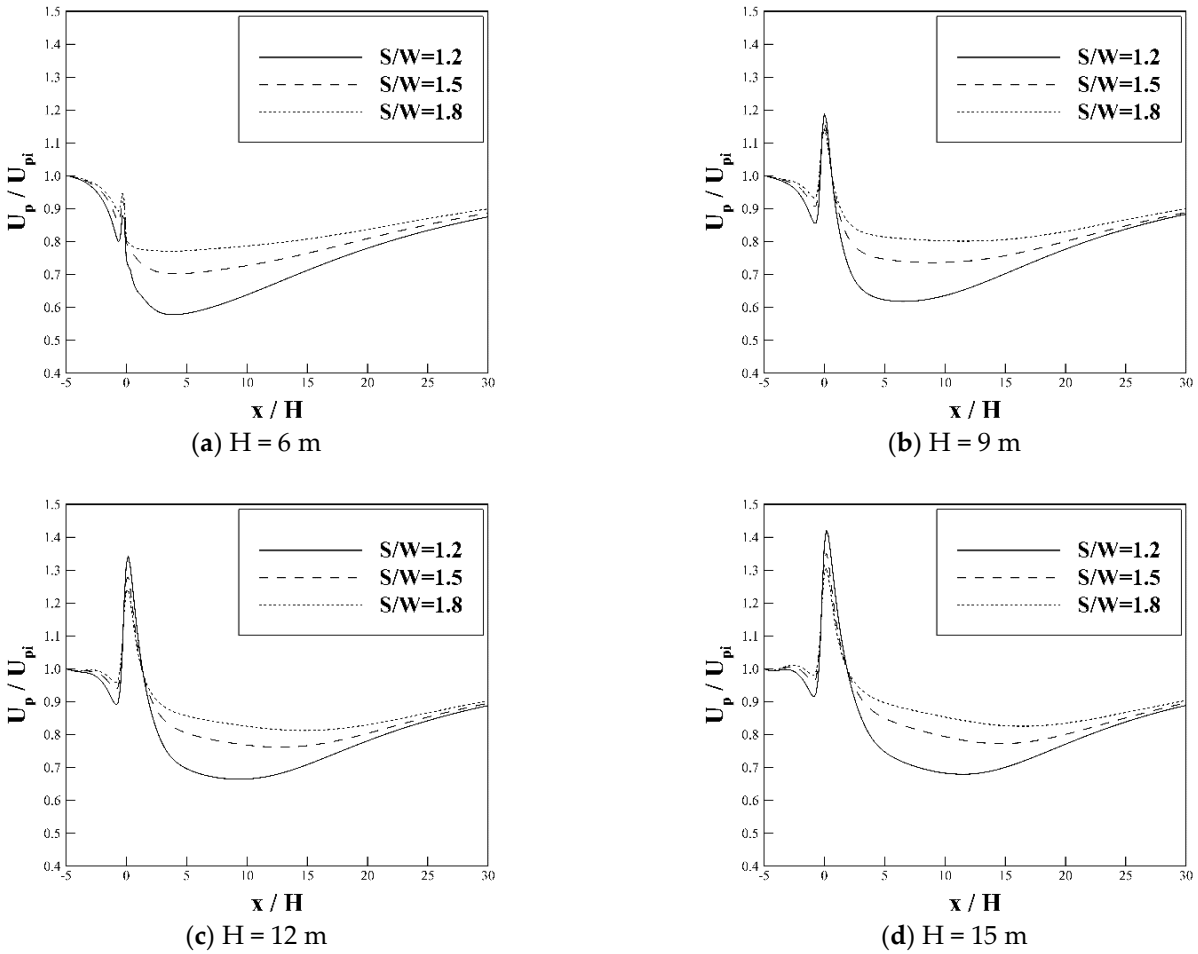
Figure 13. *Cont.*



(**c**) S/W = 1.8

Figure 13. Pedestrian wind speed contours for different tree spaces (H = 15 m).

According to the predicted results in Figures 10–13, the stream-wise variations of pedestrian-level wind were further analyzed by taking averages along the across-wind direction. Figure 14 illustrates the patterns of the normalized mean stream-wise variations with respect to different tree space ratios (S/W) at different tree heights, where U_p and U_{pi} (=8.63 m/s) are the averaged wind speed and the starting wind speed of the oncoming flow, respectively, at a height of 2 m. These variation tendencies essentially quantitatively indicate the downstream shelter effect corresponding to different tree heights and spaces. In all cases, maximum values were found near the locations of the trees. Downstream of the locations of the local speed maxima, the cross-sectional averaged wind speeds decreased significantly until minimum values were reached. Further downstream, the wind speeds tended to recover gradually, far downstream.



(**a**) H = 6 m (**b**) H = 9 m

(**c**) H = 12 m (**d**) H = 15 m

Figure 14. Stream-wise variations of averaged pedestrian wind speeds at different tree heights.

By examining the magnitudes of the maximum pedestrian wind speeds at different tree heights and spaces, Figure 15 shows that the magnitude of the local wind speed maxima appears insensitive to the change of the tree distance when H = 6 m. When the trees are taller, however, the value of the maximum wind speed becomes greater as the tree height increases or the tree space decreases. On the other hand, Figure 16 illustrates the locations and magnitudes of the downstream minimum pedestrian wind speeds. In the cases of 6 m tree height, the location of minimum wind speed appears nearly independent of the tree space. When the tree becomes taller, the minimum value occurs further downstream with increases of the tree height and tree space. Meanwhile, the magnitude of the minimum wind speed generally increases as the tree height increases or the tree space increases.

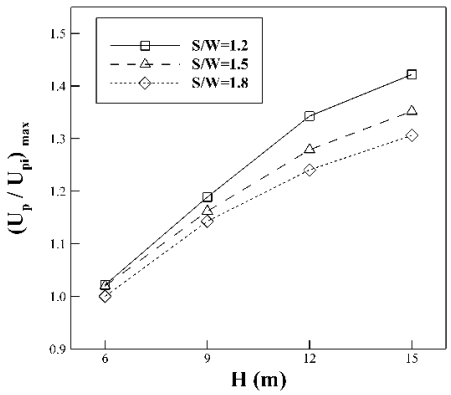
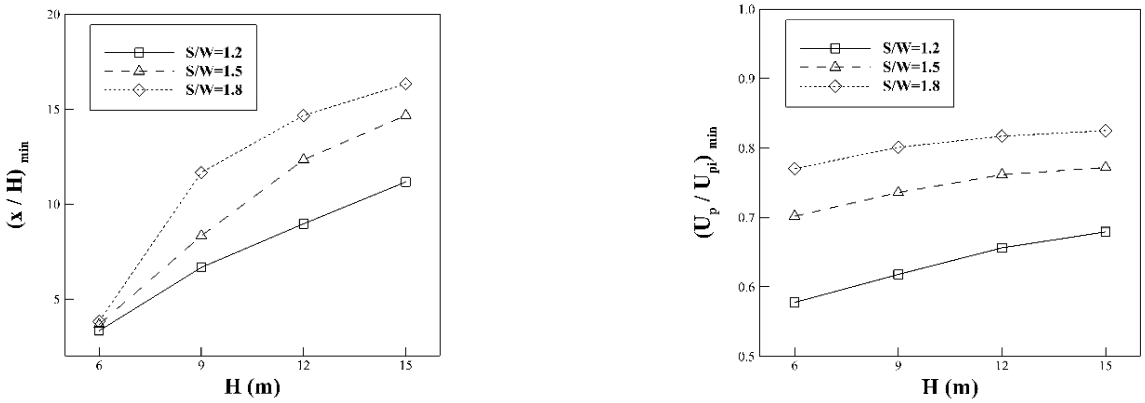


Figure 15. Normalized magnitudes of maximum pedestrian wind speeds.



(**a**) Location (**b**) Magnitude

Figure 16. Locations and magnitudes of minimum pedestrian wind speeds.

9. Discussions

In the western coastal regions of Taiwan, many land development projects have been undertaken on certain reclaimed lands. Due to the action of strong winds that occur in the fall and winter seasons, the strength of near-ground wind speed often becomes great and thus degrades the comfort of local residents. To improve the outdoor living environment of humans on certain reclaimed lands, planting row trees has become an efficient method to reduce ground wind speeds. For the purpose of wind reduction, the appropriate selections of row-tree arrangements require more extensive studies.

The problem of wind past row trees is rather complicated since it involves a great deal of uncertainty, examples of this include concerned sheltered area, local meteorology, topography, the geometrical (shape, height) and physical properties (crown density) of trees, and so on. Even for a specific type of tree, the height, crown shape, and crown density can change at different growth ages or in different seasons. Depending on the

protected region of concern, on the other hand, the selection of row-tree arrangements may be different. Therefore, to achieve definite guidelines for row-tree planting that are applicable in all real cases is somewhat impractical. Instead, by taking the problem with commonly adopted types of trees as a typical example, performing systematic analyses on the general behavior and tendency of flows behind the row trees, to achieve applicable knowledge to help the understandings of landscape planners, is considered one of the major goals of this study.

Since *Koelreuteria henryi* is one of the most popular landscape trees adopted for row trees in Taiwan, it was selected as the example tree in the present study. By conducting additional analyses of the flow results, effects due to the changes in tree heights and tree spaces were extensively examined. The achieved quantitative information can be referenced in other cases of row trees with similar crown shapes and crown properties. There have been typical discussions and proposals [21–26] made available regarding the evaluations of the extent of pedestrian comfort under the action of wind. Accordingly, the quantitative information of the resulting spatial distributions of the pedestrian-level wind speeds at different tree heights and tree spaces (Figures 10–13), as well as the corresponding stream-wise speed variations (Figure 14), can be readily used to proceed with further shelter effect assessments and pedestrian comfort evaluations.

In the present study, systematic analyses were carried out based on the results of numerical flow computations. Different from other previous related studies, investigations concentrated on the wind fields behind the row trees at the pedestrian ground level. In cases with different applicable ground levels of downstream flows with different tree species, the applicability of the presented results may be limited. However, the executed procedure of the analyses should be applicable to similar related studies of wind flows behind trees

10. Conclusions

The aims of this study were to explore the features of flows behind row trees, which are beneficial to understanding landscape planning regarding ground wind protections, and to assess downstream wind shelter effects due to changes in tree heights and tree spaces on a systematic basis. Accordingly, the wind flow past a line of evenly-spaced row trees in an open territory was numerically investigated. By taking *Koelreuteria henryi* as the species of trees, the general behaviors of the flow behind the trees with various tree heights and tree spaces has been extensively discussed.

In the present study, tree heights and tree spaces varied from 6 m to 15 m and 1.2 to 1.8 crown widths, respectively, which should cover common reasonable ranges of practical row-tree planting. Therefore, the resulting wind fields at the pedestrian level also provided quantitative information to help in the assessment of the wind shelter effect and pedestrian comfort evaluation. In other cases, with similar crown shapes and properties for row trees, these results are considered referenceable and can be readily used to estimate the efficiency of wind protection by a selected row tree arrangement in the preliminary planning stage.

Finally, a demonstrative procedure of flow analyses behind row trees was presented. The steps of execution, including the determination of the crown factor (C_{Da}), the numerical treatments of the crown retardation effects in the flow computations, and the assessments of the shelter effect behind row trees, can be used by future researchers and professionals dealing with such wind-flow problems.

Author Contributions: Conceptualization, F.-M.F. and M.-H.C.; instrument installation, J.-C.C. and C.-Y.C.; investigation, J.-C.C. and M.-H.C.; formal analysis, F.-M.F., Y.-C.L. and M.-H.C.; writing—review and editing, M.-H.C. and F.-M.F. All authors have read and agreed to the published version of the manuscript.

Funding: This research was funded by the Ministry of Science and Technology in Taiwan (Grant No. MOST 109-2221-E-005-003).

Informed Consent Statement: Informed consent was obtained from all subjects involved in the study.

Data Availability Statement: Not available.

Acknowledgments: The computation resource was provided by the National Center for High-Performance Computing in Taiwan.

Conflicts of Interest: The authors declare no conflict of interest.

References

1. American Society of Civil Engineers (ASCE). *Minimum Design Loads for Buildings and Other Structures*; American Society of Civil Engineers: Reston, VA, USA, 2017.
2. Finnigan, J. Turbulence in Plant Canopies. *Annu. Rev. Fluid Mech.* **2000**, *32*, 519–571. [CrossRef]
3. Raupach, M.R.; Coppin, P.A.; Legg, B.J. Experiments on Scalar Dispersion within a Model Plant Canopy. Part I: The Turbulence Structure. *Bound.-Layer Meteorol.* **1986**, *35*, 21–52. [CrossRef]
4. Raupach, M.R.; Antonia, R.A.; Rajagopalan, S. Rough-Wall Turbulent Boundary Layers. *Appl. Mech. Rev.* **1991**, *44*, 1–25. [CrossRef]
5. Mihailovic, D.T.; Lalic, B.; Rajkovic, B.; Arsenic, I. A Roughness Sublayer Wind Profile above Non-uniform Surface. *Bound.-Layer Meteorol.* **1999**, *93*, 425–451. [CrossRef]
6. Massman, W. A Comparative Study of some Mathematical Models of the Mean Wind Structure and Aerodynamic Drag of Plant Canopies. *Bound.-Layer Meteorol.* **1987**, *40*, 179–197. [CrossRef]
7. Novak, M.D.; Warland, J.S.; Orchaansky, A.L.; Ketler, R.; Green, R. Wind Tunnel and Field Measurements of Turbulent Flow in Forests. Part I: Uniformly Thinned Stands. *Bound.-Layer Meteorol.* **2000**, *95*, 457–495. [CrossRef]
8. Boldes, U.; Colman, J.; Maranon, D.L.J. Field Study of the Flow behind Single and Double Row Herbaceous Windbreaks. *J. Wind Eng. Ind. Aerod.* **2001**, *89*, 665–687. [CrossRef]
9. Flesch, T.K.; Wilson, J.D. Wind and Remnant Tree Sway in Forest Cutblocks. I. Measured Winds in Experimental Cutblocks. *Agric. For. Meteorol.* **1999**, *93*, 229–242. [CrossRef]
10. Flesch, T.K.; Wilson, J.D. Wind and Remnant Tree Sway in Forest Cutblocks. II. Relating Measured Tree Sway to Wind Statistics. *Agric. For. Meteorol* **1999**, *93*, 243–258. [CrossRef]
11. Uno, I.; Ueda, H.; Wakamatsu, S. Numerical Modeling of the Nocturnal Urban Boundary Layer. *Bound.-Layer Meteorol.* **1989**, *49*, 77–98. [CrossRef]
12. Hiraoka, H. Modelling of Turbulent Flows within Plant/Urban Canopies. *J. Wind Eng. Ind. Aerod.* **1993**, *46-47*, 173–182. [CrossRef]
13. Shaw, R.H.; Schumann, U. Large-eddy Simulation of Turbulent Flow Above and within A Forest. *Bound.-Layer Meteorol.* **1992**, *61*, 47–64. [CrossRef]
14. Wilson, J.D.; Flesch, T.K. Wind and Remnant Tree Sway in Forest Cutblocks. III. A Windflow Model to Diagnose Spatial Variation. *Agric. For. Meteorol.* **1999**, *93*, 259–282. [CrossRef]
15. Su, H.B.; Shaw, R.H.; Pawu, K.T.; Moeng, C.H.; Sullivan, P.P. Turbulent Statistics of Neutrally Stratified Flow within and above a Sparse Forest from Large-Eddy Simulation and Field Observations. *Bound.-Layer Meteorol.* **1998**, *88*, 363–397. [CrossRef]
16. Patton, E.G.; Davis, K.J. Decaying Scalars Emitted by a Forest Canopy: A Numerical Study. *Bound.-Layer Meteorol.* **2001**, *100*, 91–129. [CrossRef]
17. Watanabe, T. Large Eddy Simulation of Coherent Turbulence Structures Associated with Scalar Ramps over Plant Canopies. *Bound.-Layer Meteorol.* **2004**, *112*, 307–341. [CrossRef]
18. Sladek, I.; Bodnar, T.; Kozel, K. On a Numerical Study of Atmospheric 2D and 3D-Flows over a Complex Topography with Forest Including Pollution Dispersion. *J. Wind Eng. Ind. Aerod.* **2007**, *95*, 1424–1444. [CrossRef]
19. Fang, F.M.; Liang, T.C.; Chung, C.Y.; Li, Y.C. On the Simulation of Flow around Discrete Coniferous Trees. *J. Chin. Inst. Eng.* **2015**, *38*, 665–674. [CrossRef]
20. Schomaker, M.E.; Zarnoch, S.J.; Bechtold, W.A.; Latelle, D.J.; Burkman, W.G.; Cox, S.M. *Crown-Condition Classification: A Guide to Data Collection and Analysis*; Technical Report SRS–102; United States Department of Agriculture Forest Service, Southern Research Station General: Asheville, NC, USA, 1975.
21. Penwarden, A.D. Acceptable Wind Speeds in Towns. *Build. Sci.* **1973**, *8*, 259–267. [CrossRef]
22. Isyumov, N.; Davenport, A.G. The Ground Level Wind Environment in Build-up Areas. In *Proceedings of the 4th International Conference on Wind Effects on Buildings and Structures*; Cambridge University Press: Cambridge, UK, 1975; pp. 403–422.
23. Hunt, J.C.R.; Poulton, E.C.; Mumford, J.C. The Effects of Wind on People: New Criteria Based on Wind Tunnel Experiments. *Build. Environ.* **1976**, *11*, 15–38. [CrossRef]
24. Melbourne, W.H. Criteria for Environmental Wind Conditions. *J. Wind Eng. Ind. Aerod.* **1978**, *3*, 241–249. [CrossRef]
25. Durgin, F.H.; Chock, A.W. Pedestrian Level Winds: A Brief Review. *J. Struct. Div.-ASCE.* **1982**, *108*, 1751–1767. [CrossRef]
26. Arens, E.; Ballanti, D.; Bennett, C.; Guldman, S.; White, B. Developing the San Francisco Wind Ordinance and Its Guidelines of Compliance. *Build. Environ.* **1989**, *24*, 297–303. [CrossRef]